REFLUX SOLAR RECEIVER DESIGN CONSIDERATIONS*

SAND91-1267C

R.B. Diver

Sandia National Laboratories
Albuquerque, NM 87185

Abstract

Reflux heat-pipe and pool-boiler receivers are being developed to improve upon the performance and life of directly-illuminated tube receiver technology used in previous successful demonstrations of dish-Stirling systems.

The design of a reflux receiver involves engineering tradeoffs. In this paper, on-sun performance measurements of the Sandia pool-boiler receiver are compared with results from the reflux receiver thermal analysis model, AEETES. Flux and performance implications of various design options are analyzed and discussed.

Introduction

Dish-Stirling solar energy systems have previously demonstrated the highest solar-to-electric conversion efficiencies of any solar conversion device. [1] Because they also have the potential for long life and low cost, dish-Stirling technology development is being supported by the U.S. Department of Energy (DOE) and industry. [2,3] For several years, technology development has concentrated on improved components. Stirling engine development has featured free-piston and advanced kinematic Stirling engines; concentrator development has emphasized single-element and faceted stretched-membrane dishes; and receiver development has pursued liquid-metal reflux heat-pipe and pool-boiler receivers. [2]

In a reflux solar receiver, a liquid metal such as sodium (Na), potassium (K), or a combination (NaK), is used as an intermediate heat transfer fluid between a solar-heated concave spherical absorber and the heater tubes of a Stirling engine, Fig. 1. The liquid metal is returned to the absorber by gravity (refluxing). In the reflux heat-pipe receiver, liquid metal is distributed over the absorber by capillary forces in a wick. In the reflux pool-boiler receiver, liquid metal distribution is provided by sufficient inventory to submerge the absorber in all orientations. The engine heater tubes always remain in the vapor space above the pool. Both types of reflux receivers allow independent design and optimization of the receiver and engine, result in isothermal operation of Stirling engine heater tubes, and permit the addition of a fossil fuel heat source (hybridization). During normal operation, heat-transfer coefficients of the evaporating liquid metal in both cases are high, resulting in nearly uniform solar absorber temperatures.

* This work was supported by the U.S. Department of Energy under contract DE-AC04-76-DP00789.

The design of reflux solar receivers involves engineering tradeoffs of factors that affect survivability, cost, life, and performance. Although many issues are unique to specific designs, reflux receiver geometries tend to be similar. This is because pressure stresses (caused by pressure differences between atmospheric and internal vacuum) and thermal stresses (caused by the thermal gradient though the absorber surface) generally dictate thin spherical absorbers with hemispherical or nearly hemispherical geometries. The size of reflux receivers is also limited by capillary pumping limitations in heat pipes and, to a lesser extent, by liquid metal inventory considerations in pool boilers. And while reducing receiver size is also desirable because it reduces cost and cavity convection heat loss, it also increases incident solar flux intensities. Depending on the design, materials, and operating conditions, the peak flux capability of heat-pipe and pool-boiler receivers is limited and is usually an overriding design consideration.

In this paper, reflux receiver design parameters are discussed and the optical simulation model, CIRCE2, and the reflux receiver thermal performance model, AEETES, are used to explore the flux and performance implications. The designs used in the simulations are based on the Sandia pool-boiler receiver which was tested on-sun. Performance simulation results are compared with measurements. Results from the simulations are parametrically extended to various design options and are discussed.

Reflux Receiver Performance Parameters

The performance of solar receivers is dependent on a number of factors. In Table 1 the variables that affect the performance of reflux receivers are categorized and listed. In general, receiver performance is a function of (1) receiver geometry, (2) receiver materials properties, (3) environmental parameters, and (4) system parameters, i.e., variables that are dictated by other components and/or system considerations. Because aperture diameter is established by the concentrator's performance characteristics, it is considered to be a system parameter, rather than a receiver geometry parameter.

The parameters generally used to characterize receiver performance are receiver efficiency (η_r) and heat loss (Q_l). Receiver efficiency is a function of heat loss and input power (Q_i). Input power is defined here as the power delivered by the concentrator through the aperture. Output power (Q_o) is the power delivered to the engine.

$$\eta_r = \frac{Q_i - Q_l}{Q_i} = \frac{Q_o}{Q_i} \qquad \text{(eqn. 1)}$$

Since heat loss (Q_l) is much less dependent on input power (Q_i) than receiver efficiency (η_r), heat loss is the most useful performance parameter.

Heat losses from solar receivers are comprised of (1) solar energy reflected from the receiver (Reflection), (2) infrared radiation emitted from the

receiver (Reradiation), (3) energy conducted through the insulation (Conduction), and (4) energy convected from the receiver (Convection). Of these, convection is the most difficult to predict.

Performance Measurement Results

The Sandia pool-boiler receiver was primarily designed to establish the operational feasibility, characteristics, and limitations of the reflux pool-boiler receiver concept. It also provided an opportunity to assess reflux receiver performance in a controlled experiment. Unlike other dish receivers, which have only been evaluated as part of a system, the Sandia pool-boiler receiver was designed to operate with a gas-gap cold-water calorimeter. [4] Since the gas-gap cold-water calorimeter's instrumentation was identical to that used to characterize test bed concentrator #1 (TBC-1), relatively accurate measurement of receiver performance was feasible. Measured heat loss was determined by subtracting the power delivered by the receiver to the cold-water gas-gap calorimeter from the power provided by TBC-1 to the same size aperture on a cold-water calorimeter.

The cavity geometry of the Sandia pool-boiler receiver is shown in Fig. 2. The spherical absorber geometry was selected primarily for structural reasons and utilized a 0.414 m (16.3 inch) diameter spherical absorber with a 0.219 m (8.62 inch) radius of curvature. The sphere half angle was therefore about 71°. The cavity design utilized a 0.22 m (8.66 inch) diameter aperture and an oxidized SS316 sidewall. [4] Since the TBCs have a rim angle of approximately 45°, the design position of the absorber rim is 0.097 m (3.82 inch) behind the aperture/focal plane to match the cavity side-wall angle with the concentrator rim angle and avoid directly illuminating the un-cooled cavity sidewall.

The size of the absorber and cavity geometry were based, to a large extent, on peak flux considerations. An objective for this design was to operate at relatively high peak flux intensities, approximately 70 W/cm^2, previously demonstrated in bench scale tests. [5] For comparison, the Stirling Technology Co. conceptual design for a 75 kW_t pool-boiler receiver with a similar geometry used an absorber diameter of 0.508 m (20 inch) and a peak flux intensity of approximately 46 W/cm^2. [6] The Thermacore, Inc. heat pipe receiver used on the CPG 5 kW_e dish-Stirling system is a 0.406 m (16 inch) diameter hemisphere. The predicted peak flux intensity is less than 30 W/cm^2 at 30 kW_t with a well aligned LEC-460 concentrator. [7]

Figure 3 is the CIRCE2 predicted incident solar flux distribution for the design configuration. CIRCE2 is an improved version of CIRCE [8] and accounts for (1) dish and facet geometry, (2) facet curvature, (3) facet alignment, (4) facet shading and blockage, and (5) receiver geometry. [9] The peak incident flux is 73 W/cm^2 for the design condition with 75 kW_t incident power.

TBC-1 was characterized with a cold-water calorimeter between July 12 and August 3, 1989. [10] Measurements were made with the concentrator in various states of cleanliness and at 1/2, 3/4, and full power. Normalized power delivered by TBC-1 through a 22-cm (8.7 inch) diameter aperture ranged from 64.1 kW_t with dirty mirrors, about 65.0 kW_t with "intermediate" dirty mirrors, to 66.6 kW_t with clean mirrors. Opening the calorimeter aperture to 0.60 m (24 inch) increased normalized input power by only 0.3 kW. The

accuracy of the Delta-T Company differential temperature transducer was 0.04°C resulting in better than 1% accuracy for typical ΔTs of over 10°C. The accuracy of the Flow Technology Company turbine flow meter and Epply direct-normal-insolation pyrheliometer were each better than 1%. Periodic checks of the turbine flow meter's calibration during operation with a bucket, scale, and stop watch confirmed the reported flow-meter accuracy. The overall power-measurement accuracy was determined to be about 0.8 kW_t. [10]

Because of (1) the degraded performance of TBC-1, (2) the objective to operate at high incident peak flux intensities, and (3) concerns about the vulnerability of the absorber's rim weld in a concentrator mis-track condition, the absorber was moved 2 cm (0.79 inch) closer to the aperture than shown in Fig. 2 for the on-sun tests.

The performance results presented in Table 2 are for conditions in which the receiver had been operated for at least one hour (to minimize start-up transient heating) and which had generally operated stablily for a period of at least 10 minutes. Each of the entries represents the average of 25 measurements over a 6 minute period. The 13:04, May 9, 1990 condition is an exception. It is the mean of 18 data points over a 4 minute period.

A source of input-power uncertainty was from estimating the level of mirror cleanliness. Based on visual observations of mirror cleanliness, input power was estimated to be 64.4 kW_t normalized to 1-kW/m^2 direct normal insolation for the results in Table 2. Mirrors were not washed after August 2, 1989. For the 1989 data, the estimated uncertainty in normalized input power due to mirror cleanliness was 0.6 kW_t. The root-sum-square method uncertainty in receiver input power is therefore about 1 kW_t. (1 kW_t = $(0.8^2 + 0.6^2)^{0.5}$, where 0.8 is the measurement uncertainty from reference [10].) For the May 1990 results, input power uncertainty was assumed to increase to about 1.2 kW_t because of the additional time period following TBC calorimetry.

Unfortunately as a result of a failure of the absorber during a unique hot-restart condition on May 30, 1990, the pool-boiler receiver was not completely characterized for performance. [11] The bucket, scale, and stop-watch technique was not utilized to check the flow meter's calibration until November 15, 1989. In that check, the flow meter was found to be in error by about 4%. Correcting the flow-meter measurements for the "all day" test of October 19, 1989, based on the calibration check of November 15, 1989, provides four of the performance measurements presented in Table 2. Because of the flow-measurement uncertainty in this data, the receiver output power uncertainty was estimated to be about 3.0 kW_t. Data taken during the period in which flow was calibrated on November 15, 1989 provides the most accurate heat-loss measurements. Heat loss during this period was just less than 10 kW_t. The low elevation angle (about 25°) and the high wind speed (over 5 m/sec) probably contributed to the relative high heat loss.

Tests in May of 1990, just prior to the failure, provided additional performance data. In these tests a factory calibrated flow meter placed on the inlet line provided more accurate water flow measurement. The aperture was also opened to 26 cm (10.2 inch) diameter. Despite the enlarged aperture diameter for these runs, heat loss was measured to be less than on November 15, 1989 -- probably because of the higher elevation angles and

therefore lower convection loss. During the May 18 testing the inlet flow meter was calibrated with the bucket, scale, and stopwatch technique. All of the May performance test results are based on the May 18 calibration.

Reflux Receiver Performance Analysis

Numerical models have been developed at Sandia to evaluate the thermal performance of reflux receivers. A finite-control-volume (FCV) model was developed and used to evaluate thermal performance and potential weld over heating of the Sandia pool-boiler receiver. A simpler and easier-to-use thermal-resistance (TR) model was also developed to simulate reflux receiver performance and to make parametric studies. [12,13]

The TR model, recently named AEETES (in Greek mythology AEETES was the brother of CIRCE), has been used to explore the performance implications of some of the variables in Table 1. The details of AEETES are presented in reference [13] in the TR Model section. The current AEETES model calculates surface temperature distributions and heat loss of axisymmetrical cavity receivers. Recent improvements to AEETES includes an option to model asymmetrical flux and temperature distributions. For the results presented here, surface elements are specified as annular ring-shaped elements which form basic geometric shapes, e.g., conics, cylinders, spheres, and disks (consistent with CIRCE2). The analysis of radiation and the resulting temperature distributions are therefore two-dimensional axisymmetric. Input incident flux from CIRCE2 is averaged over the azimuthal dimension to produce a one-dimensional radial distribution. Multiple reflection of solar flux and reflection and reradiation of infrared energy between the ring shaped elements is taken into account. Surfaces are assumed to be diffuse and gray with separate solar and infrared radiation properties. The aperture is treated as a black surface with a temperature 6°C less than ambient. [14]

One-dimensional heat conduction models are used to calculate conduction heat loss (through the cavity sidewalls) and heat delivered to the sodium (through the absorber). Depending on the geometry, the one-dimensional conduction equation for each surface element is written in terms of planar, cylindrical, or spherical thermal resistances. Cavity convection coefficients for each surface can be arbitrarily specified or determined from correlations. For these analyses, the correlation recommended by Stine [15], which accounts for cavity geometry, aperture diameter, cavity and ambient temperatures, and sun-elevation angle, are utilized. Energy balance equations on each element are used to iteratively solve for the surface temperature distribution. An iteration conversion criterion of 0.001°C change per iteration was used.

Insulation geometries for all of the analyses were assumed to be cylindrical on the outside diameter (surrounding the sidewall), with a minimum thickness at the intersection of the absorber and sidewall of 15.24 cm (6 inch). The convection coefficient from the insulation housing to the surrounding air was assumed to be 20 W/m^2-K. The insulation conductivity was assumed to be 0.4 W/m-K. This value is approximately four times higher than published values to account for heat loss axially through the insulation adjacent to the aperture (2-dimensional conduction), heat loss though insulation surrounding the aft dome, and to better account for radiation heat transfer

through the insulation. Conduction heat loss results (253 W in this case) should therefore be considered approximate. These results and more rigorous analyses agree in that conduction is a relatively small loss component. By comparison the FCV model predicts conduction heat loss to be about 325 W for this condition.

The convective heat transfer rate from the absorber to the sodium was assumed to be fast ($1X10^8$ W/m^2-K), essentially forcing the absorber side temperature equal to the sodium vapor temperature. In actuality, wall superheats on the order of 10°C might be expected, but are not accounted for in these analyses. The absorber temperature distribution predicted by AEETES matches the one-dimensional CIRCE2 incident solar flux distribution.

Figure 4 shows the temperature distribution and summarizes the design point efficiency and heat loss components of the Sandia pool-boiler receiver predicted by AEETES. Input parameters to AEETES are listed in Table 1. The cavity geometry and the 16 sidewall and 40 absorber ring elements used in the calculations are evident in the figure. The total receiver heat loss for the design condition depicted in Fig. 4 is 6510 W. Radiation (3180 W) is the largest source. Cavity refection (1530 W) and convection (1550 W) losses are also substantial. Sidewall temperatures of approximately 900°C are in good agreement with the experimental data. [13]

The comparisons of the measured and predicted heat loss, presented in Table 2 and plotted in Fig. 5, indicate reasonable agreement between measured data and predicted results. Measured input power, condenser temperature, sun angle, and ambient temperature were used as inputs to AEETES. Increased convection loss due to winds which are not accounted for in the convection correlation; AEETES's tendency to underpredict conduction loss; increased absorber temperature due to boiling (wall) superheat; and possible degradation of TBC-1 during the winter of 1989-1990 are some of the likely reasons for the higher measured heat loss values.

Parametric Performance Analysis

The reflux receiver thermal model, AEETES, has been used to explore operational and design variations relative to the design point geometry and conditions outlined in Table 1 and Figs. 2 and 4. Even though comparisons with experimental data indicates reason for confidence in AEETES, many of the important design variables were not exercised in the comparisons discussed above. At the same time, however, with the exception of convection, the heat transfer mechanisms are well understood. It is reasonable, therefore, to expect AEETES to provide a good relative comparison of the performance implications of design and operational changes.

Figures 6 through 8 show the effect of the system parameters on the heat loss components. As expected, heat loss from the receiver is a strong function of aperture diameter (Fig. 6) and operating temperature (Fig. 7). These are in fact key optimization variables in any solar thermal system and are largely established by concentrator and engine performance characteristics respectively. Receiver heat loss, on the other hand, (Fig. 8) is weakly dependent on the incident solar flux distribution. This is because the high heat-transfer rates associated with liquid-metal reflux

receivers essentially makes the receiver's temperature distribution independent of the flux distribution. Therefore, although it may be possible to achieve incremental improvements in receiver performance by the use of concentrators with relatively uniform flux, the primary motivation is reduced peak flux intensities. Because the current version of AEETES is one dimensional, the heat loss dependence on flux distribution may be underpredicted.

The effect of sun-elevation angle on heat loss is shown in Fig. 9. For the design point receiver at these conditions, convection heat loss is predicted to vary from 3584 W ($h = 12.84$ W/m^2-K) with the sun on the horizon to 0 W with the sun directly over head. There is a significant amount of uncertainty with the Stine correlation for this configuration and conditions. In addition, convection is strongly dependent on wind.

Figure 10 shows that increasing the absorber solar absorptivity from 0.87 (measured value for the SS316L Sandia pool-boiler receiver) to 0.91 (measured value for oxidized Haynes 230) reduces overall heat loss by about 670 W. A high solar absorptivity paint (α=0.95) can potentially reduce heat loss by about 1340 W. Even if the paint increases the thermal resistance of the absorber, performance improvements can be obtained. For example, the increased thermal resistance point on Fig. 10 is based on a paint thickness of .00254 cm (0.001 inch) and a thermal resistance of 0.4 W/m^2-K. Even though the paint increases the area-weighted average absorber temperature by about 20°C, overall heat loss is reduced by about 1100 W compared with the design condition.

AEETES indicates that the use of a white sidewall material, such as an alumina-silica ceramic (α_{solar} = 0.15, ε_{ir} = 0.8) instead of the SS316 sidewall in the current design, can reduce heat loss slightly (150 W), Fig. 11. Perhaps more importantly, sidewall temperatures can be reduced substantially and construction simplified.

Figures 12 and 13 show the flux and performance implications of receiver diameter and absorber position. Increasing receiver diameter or moving the absorber back effectively increase the cavity size and subsequent absorption of incident sunlight. At the same time, cavity area and cavity conduction and convection also increase, resulting in total heat loss minimums. The net effect of receiver diameter on heat loss for these conditions is relatively small, however, and is not an overriding consideration. The use of a high solar-absorptivity absorber material results in smaller optimum receiver diameters, because of relatively less reduction in reflection loss with size.

Figure 13 suggests that positioning the receiver back in the cavity can substantially reduce the incident peak flux intensity without seriously affecting performance. Exposing the un-cooled cavity sidewall and the vulnerable rim weld to high flux, however, is a potential problem with this approach. Survivability of these areas is of most concern during a concentrator mis-track condition. Although receiver performance decreases with mis-track angle because of increased reradiation and reflection from the sidewall, system performance is degraded mainly by reduced power through the aperture.

In Fig. 14 the peak incident solar flux intensity on the cavity sidewall predicted by CIRCE2 is presented as a function of concentrator mis-track angle and absorber position. The simulations are for a mis-track in azimuth. The peak sidewall flux intensity varies slightly with mis-track direction and is generally highest near the aperture. Peak flux intensities on the absorber gradually decrease with mis-track angle but can occur near the edge of the absorber. The highest peak sidewall flux intensity in Fig. 14 (11.2 W/cm^2 @ 4 cm & 10 mrd) is relatively low for the white refractory insulating materials suggested by sidewall absorptivity considerations, Fig. 11. The 3-dimensional radiation model option in AEETES and perhaps experimentation are required to accurately assess the survivability of high sidewall flux intensities. Given the substantial reductions in peak flux intensities that can be gained (about a 20% reduction between the design position and 4 cm back, see Fig. 13), this approach seems advisable. However, with this approach it is critical to protect the rim with high-temperature insulation.

Conclusions and Recommendations

Based on the results presented here, the high-performance potential of reflux receivers appears to be confirmed. The heat loss measurements of about 8 kW_t compare very favorably with those estimated by Advanco and JPL. [16, 17] Accounting for the higher operating temperature (800°C vs. about 750°C) and the larger aperture diameters (22 & 26 cm vs. 20 cm), the Sandia pool-boiler receiver performance was clearly at least as efficient as the United-Stirling tube receivers. The Sandia pool-boiler receiver was also not an optimized design. Based on AEETES simulations it is reasonable to expect improved performance with materials having better optical properties.

The calorimetry procedures used to characterize the Sandia pool-boiler receiver's performance provided the most accurate assessment of dish-receiver performance to date. Accurate differential temperature, water flow, and solar insolation measurement devices were key to accurate heat-loss measurements. Consistent measurements, with identical instruments, of concentrator and receiver performance was also important. More frequent calibration of the flow meter would have improved the measurement uncertainty. Calorimetry of TBC-1 following performance testing had been planned and would have further reduced heat-loss measurement uncertainty. Unfortunately damage to the concentrator resulting from the receiver failure eliminated the benefit of follow-up calorimetry.

The recently developed reflux receiver thermal analysis model, AEETES, appears to reasonably predict performance. Differences between measurements and model predictions appear to be caused by increased cavity convection due to the wind. Other possible contributions to the apparent discrepancy are an underprediction of cavity conduction loss, boiling superheat, and concentrator degradation during the winter.

Reflux receiver thermal performance is a function of many factors. Parametric studies around the Sandia pool-boiler receiver design indicate that the parameters with the most impact on receiver performance are system level parameters and are generally out of the control of the receiver designer. Two of the most significant factors, receiver aperture diameter and operating temperature, are dictated by the concentrator and engine

respectively. On the other hand, the receiver designer has freedom to alter absorber and cavity sidewall geometry and size in order to reduce peak incident solar flux without seriously affecting performance. The parametric studies also indicate that significant improvements in receiver performance can be obtained with improved absorber properties.

The use of white ceramic sidewall materials also appears to be advantageous. These analyses suggest that with adequate protection of the absorber rim area (with a white ceramic), placement of the absorber well behind the focal plane should substantially reduce absorber peak flux intensities without substantially affecting performance or survivability.

AEETES and CIRCE2 quantify some of the important reflux receiver design tradeoffs. These analyses illustrate some of the insights into receiver design that these models can provide. Continued refinement and improvement (specifically improvement of AEETES to consider asymmetric thermal conditions), validation, and use of these and similar analysis tools are strongly recommended.

Acknowledgements

This work was dependent on the talents of many people over many years. I am especially gratefully for the perseverance of V.J. Romero and R.E. Hogan on the development of CIRCE2 and AEETES respectively. The experimental results reported here also would not have been possible without the contributions of J.B. Moreno, C.E. Andraka, and T.A. Moss in building and instrumenting the pool-boiler receiver experiment and to K.S. Rawlinson and V. Dudley in implementing and recording the tests. The contributions of others, too numerous to name, were also instrumental.

References

1. Washom, B., "Parabolic Dish Stirling Module Development and Test Results," Paper No. 849516, Proceedings of the 19th IECEC, August 1984.

2. Diver, R.B., "Solar Thermal Electric Program," SOLTEC Proceedings, March 1991.

3. Bean, J.R. and I. Kubo, "Development of the CPG 5 kW Dish/Stirling System," Paper No. 906298, Proceedings of the 25th IECEC, August 1990.

4. Moreno, J.B., C.E. Andraka, R.B. Diver, W.C. Ginn, V. Dudley, and K.S. Rawlinson, "Test Results from a Full-Scale Sodium Reflux Pool-Boiler Receiver," Proceedings of the Twelfth Annual ASME International Solar Energy Conference, Miami, Fl, April, 1990.

5. Moreno, J.B., C.E. Andraka, R.B. Diver, T.A. Moss, E.L. Hoffman, and C.M. Stone, "Reflux Pool-Boiler as a Heat-Transport Device for Stirling Engines: Postmortem Analysis and Next-Generation Design," Paper No. 910519, Proceedings of the 26th Intersociety Energy Conversion Engineering Conference, Boston, MA, August 1991.

6. Stirling Technology Co., "25 kW_e Solar Thermal Stirling Hydraulic Engine System," DOE/NASA/0371-1, NASA CR-180889, National Aeronautics and Space Administration, Lewis Research Center, Cleveland, OH, January 1988.

7. Dussinger, P.M., "Design, Fabrication, and Test of a Heat Pipe Receiver for the Cummins Power Generation 5 kW_e Dish Stirling System," Paper No. 910824, Proceedings of the 26th IECEC, Boston, MA, August 1991.

8. Ratzel, A.C. and B.D. Boughton, "CIRCE.001: A Computer Code for Analysis of Point Focus Concentrators with Flat Targets," SAND86-1866, Albuquerque, NM, Sandia National Laboratories, February 1987.

9. Romero, V.J., "CIRCE2," 1992 ASME-JSES-KSES International Solar Energy Conference, Maui, HA, April 1992.

10. Rawlinson. K.S. and V. Dudley, "Test Bed Concentrator #1 Calorimetry Results," SAND89-2840, Sandia National Laboratories, Albuquerque, NM, February 1990.

11. Moreno, J.B., and C.E. Andraka, "Test Results from Bench Scale Sodium-Pool-Boiler Solar Receiver," SAND89-0899, Albuquerque, NM, Sandia National Laboratories, June 1989.

12. Hogan, R.E., R.B. Diver, and W.B. Stine, "Comparison of a Cavity Solar Receiver Numerical Model and Experimental Data," Journal of Solar Energy Engineering, Vol. 112, pp. 183-190, 1990.

13. Hogan, R.E., Jr., "Numerical Modeling of Dish-Stirling Reflux Solar Receivers," Proceedings of the 13th Annual ASME Solar Energy Conference, Reno, NV, April 1991.

14. Duffie, J.A., and W.A. Beckman, **Solar Energy Thermal Processes**, John Wiley & Sons, Inc. pg. 76, 1974.

15. Stine W.B. and C.G. McDonald, "Cavity Receiver Convection Heat Loss," Proceedings of the International Solar Energy Society, Solar World Congress 1989 Kobe, Kobe, Japan, September 1989.

16. Washom, B.J., "Vanguard 1 Solar Parabolic Dish-Stirling Engine Module Final Report," p. 87, DOE-AL-16333-2, September 1984.

17. Livingston, F.R., "Activities and Accomplishments in Dish/Stirling Electric Power System Development," DOE/JPL-1062-82, February 1985.

FIGURE CAPTIONS

Figure 1. Schematic showing the operation of reflux receivers.

Figure 2. Schematic showing the Sandia reflux pool-boiler receiver cavity geometry. The height of the cavity sidewall was reduced from 0.097 m to 0.077 m for the receiver tested.

Figure 3. CIRCE2 predicted incident solar flux for the design condition. The integrated solar power is 74.6 kW. The image is reversed left-to-right (like a mirror image) of what an observer, standing at the concentrator looking at the receiver, sees.

Figure 4. Sandia pool-boiler receiver design point temperature distribution and performance predicted by AEETES.

Figure 5. Comparison of AEETES predicted heat loss with measurements.

Figure 6. Receiver heat loss as a function of aperture diameter.

Figure 7. Receiver heat loss as a function of sodium vapor temperature.

Figure 8. Receiver heat loss as a function of incident flux distribution.

Figure 9. Receiver heat loss as a function of sun elevation angle.

Figure 10. Receiver heat loss as a function of absorber solar absorptivity.

Figure 11. Receiver heat loss and average sidewall temperature as a function of sidewall solar absorptivity.

Figure 12. Receiver heat loss and peak incident solar flux as a function of absorber diameter.

Figure 13. Receiver heat loss and peak incident solar flux as a function of spherical absorber position.

Figure 14. Peak sidewall incident flux as a function of absorber position (relative to design) and concentrator mis-track.

Table 1. Reflux Receiver Thermal Performance Parameters

Table 2. Sandia Pool Boiler Receiver Performance Summary

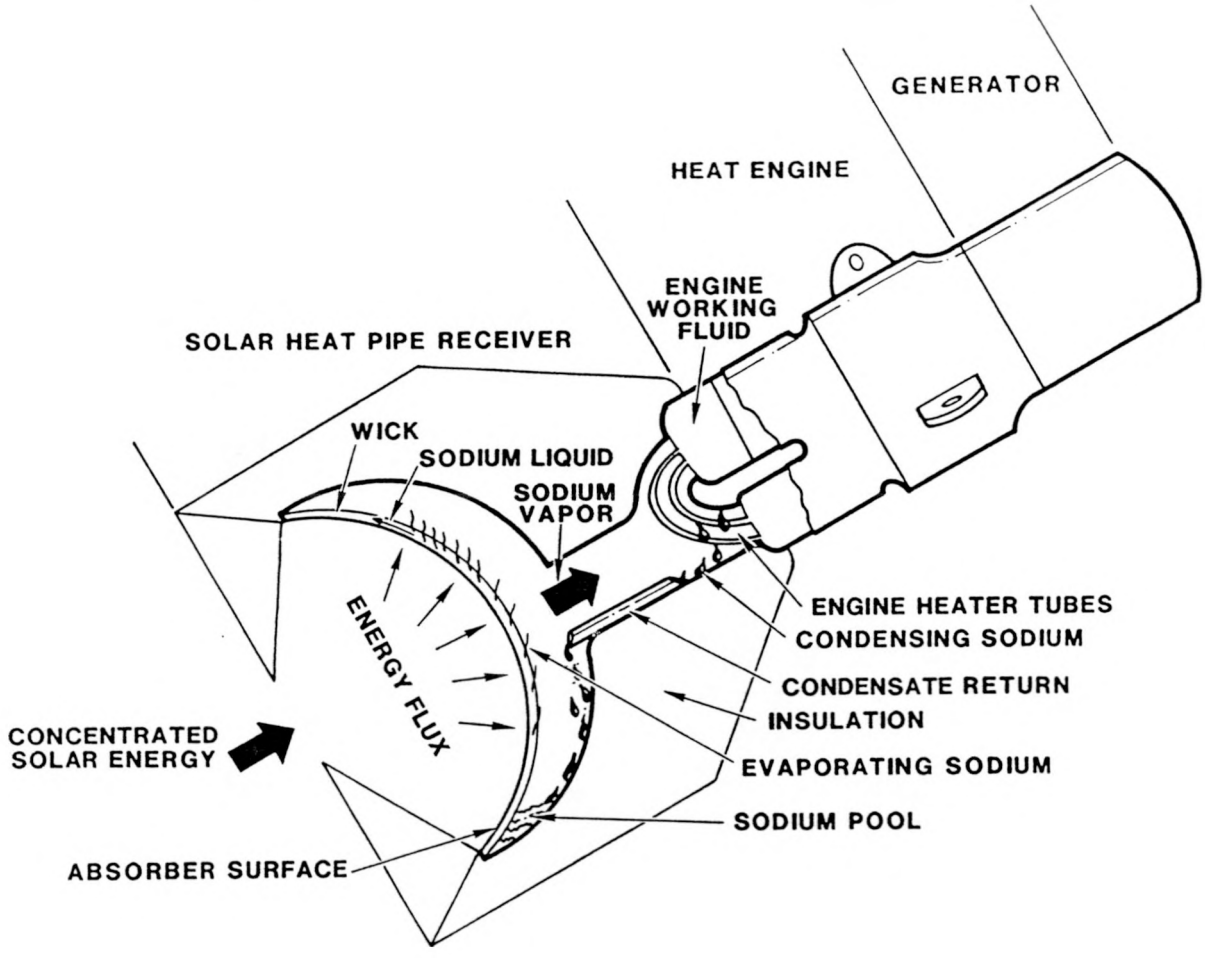
GENERATOR
HEAT ENGINE
ENGINE WORKING FLUID
SOLAR HEAT PIPE RECEIVER
WICK
SODIUM LIQUID
SODIUM VAPOR
ENERGY FLUX
ENGINE HEATER TUBES
CONDENSING SODIUM
CONDENSATE RETURN
INSULATION
EVAPORATING SODIUM
CONCENTRATED SOLAR ENERGY
SODIUM POOL
ABSORBER SURFACE

Fig 1

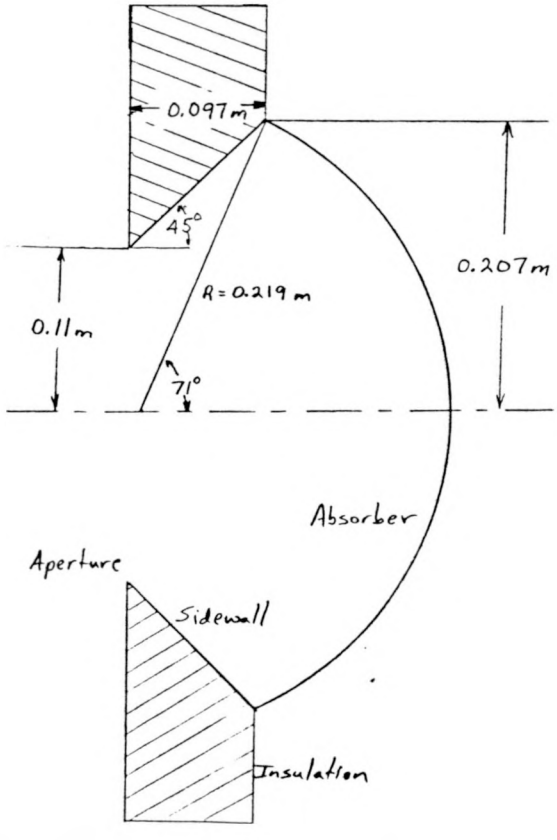
0.097m
45°
0.207m
R = 0.219 m
0.11m
71°
Absorber
Aperture
Sidewall
Insulation

Fig 2

Sandia Pool-Boiler Receiver
CIRCE2 Predicted Incident Flux
Design Conditions
74.6 kW Integrated Power

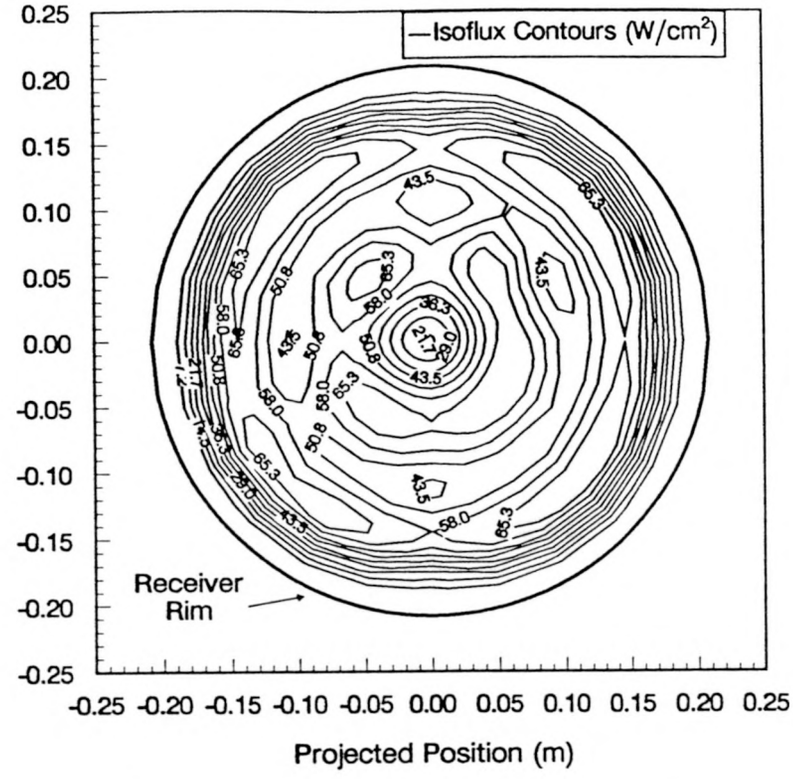

Fig 3 PB75KWD

Reflux Receiver Temperature Distribution
Sandia 16.3" Diameter Absorber

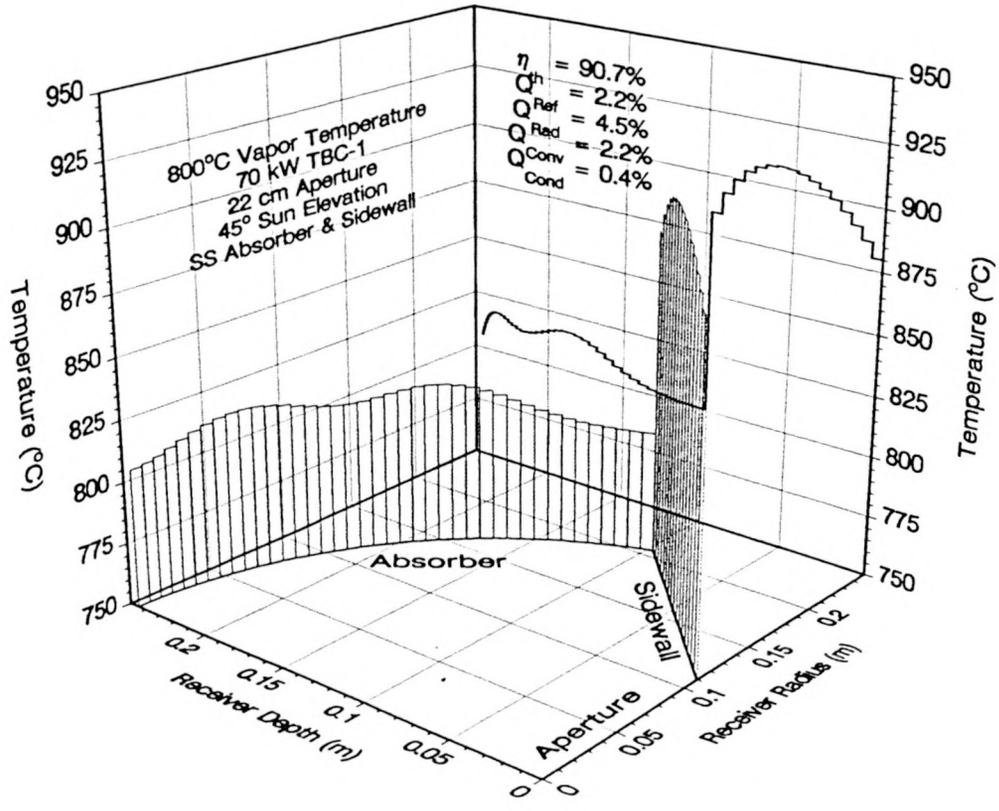

Fig 4

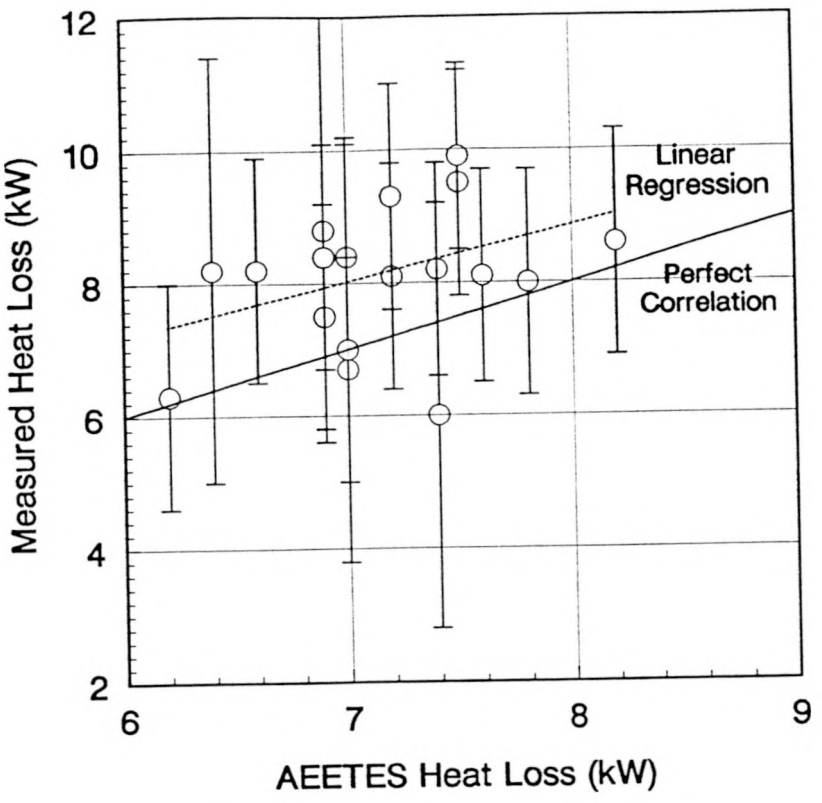

Fig 5 PBLOSS

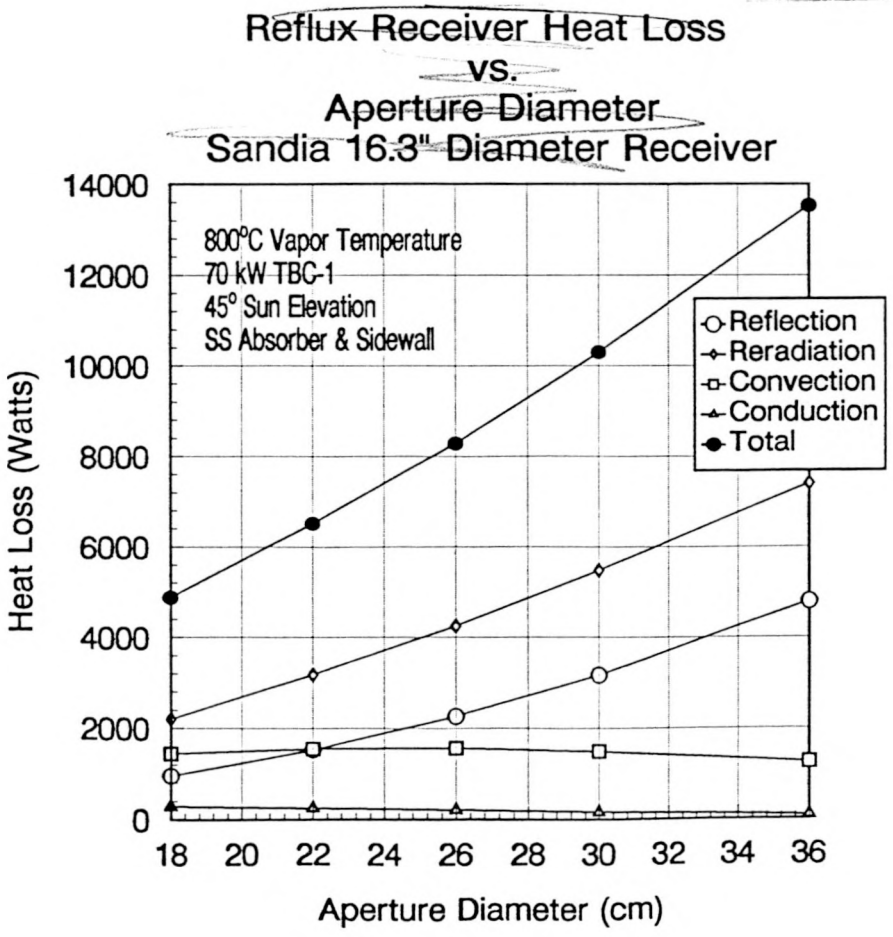

Fig 6

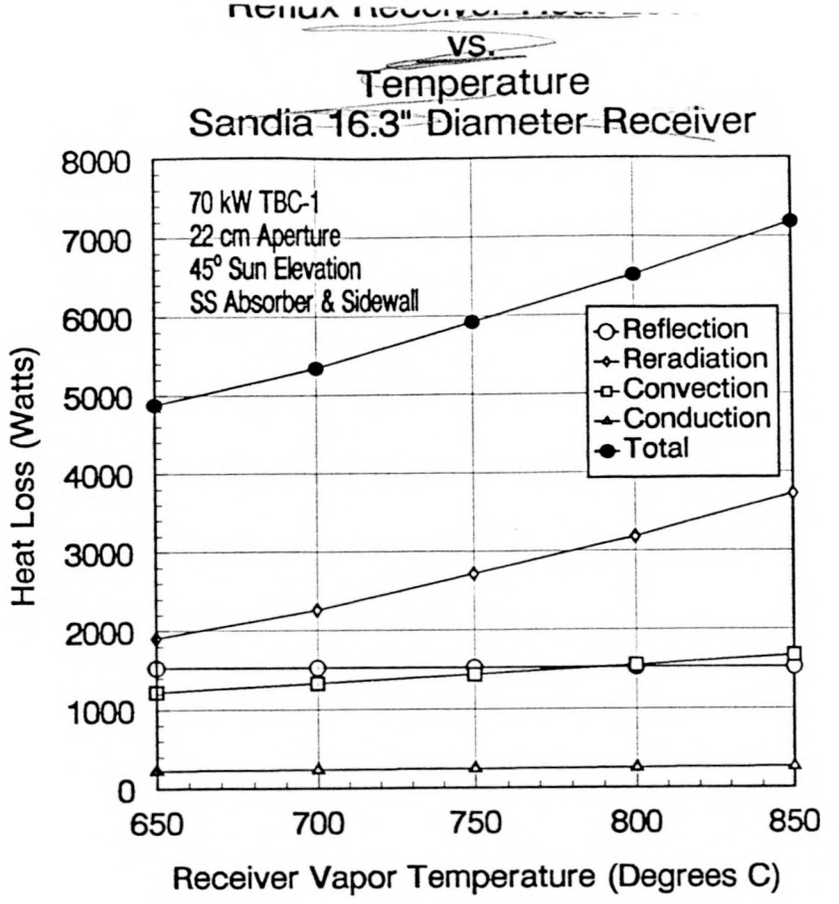

Fig 7 VI_TEMP

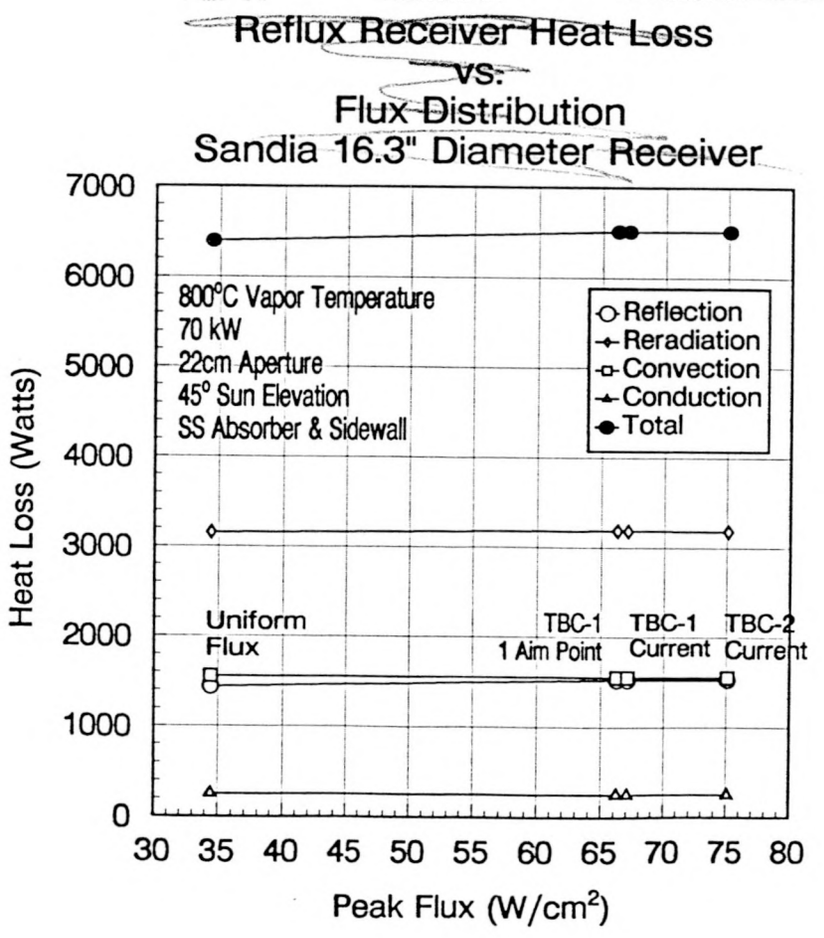

Fig 8

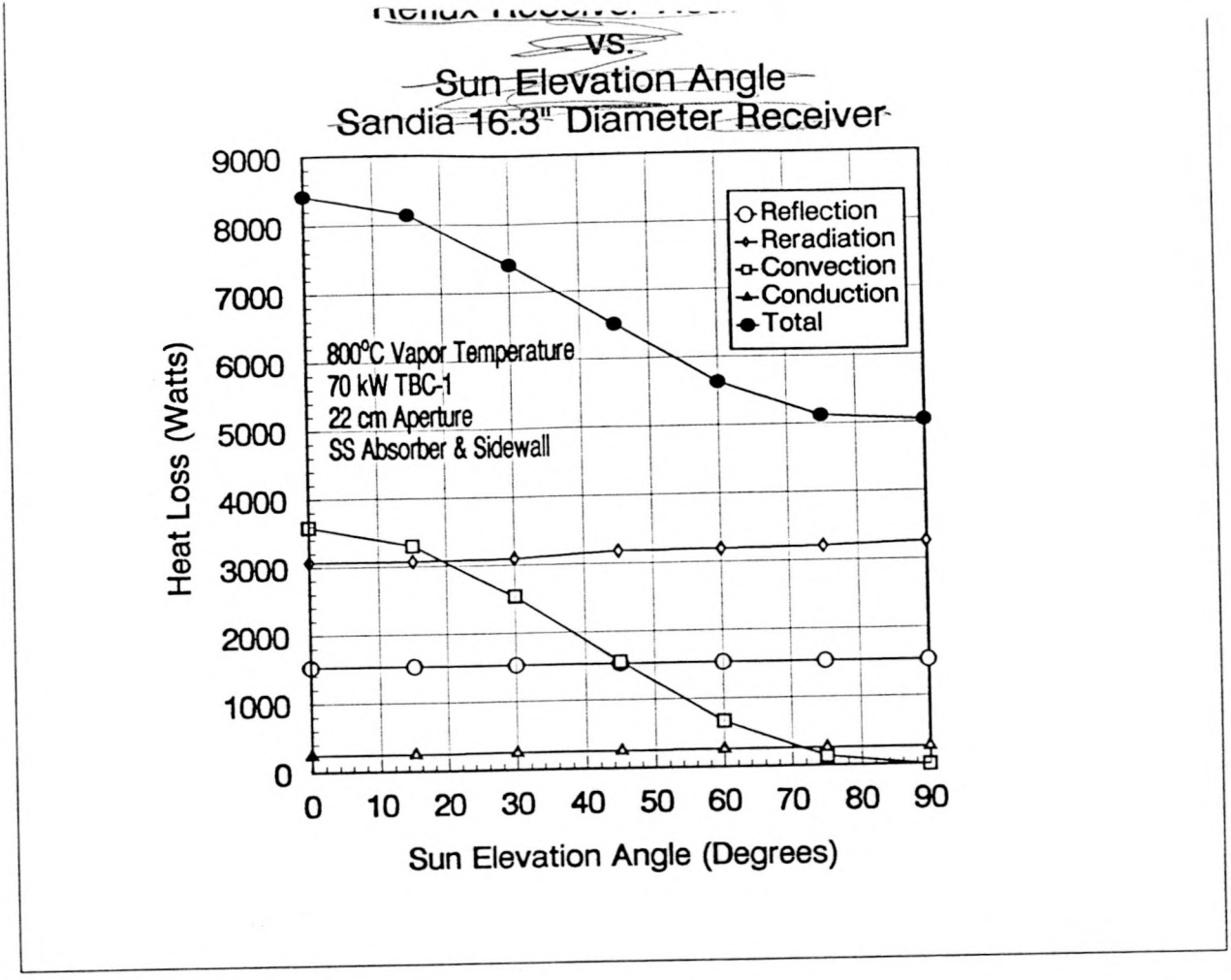

Fig 9 V_SUNELA

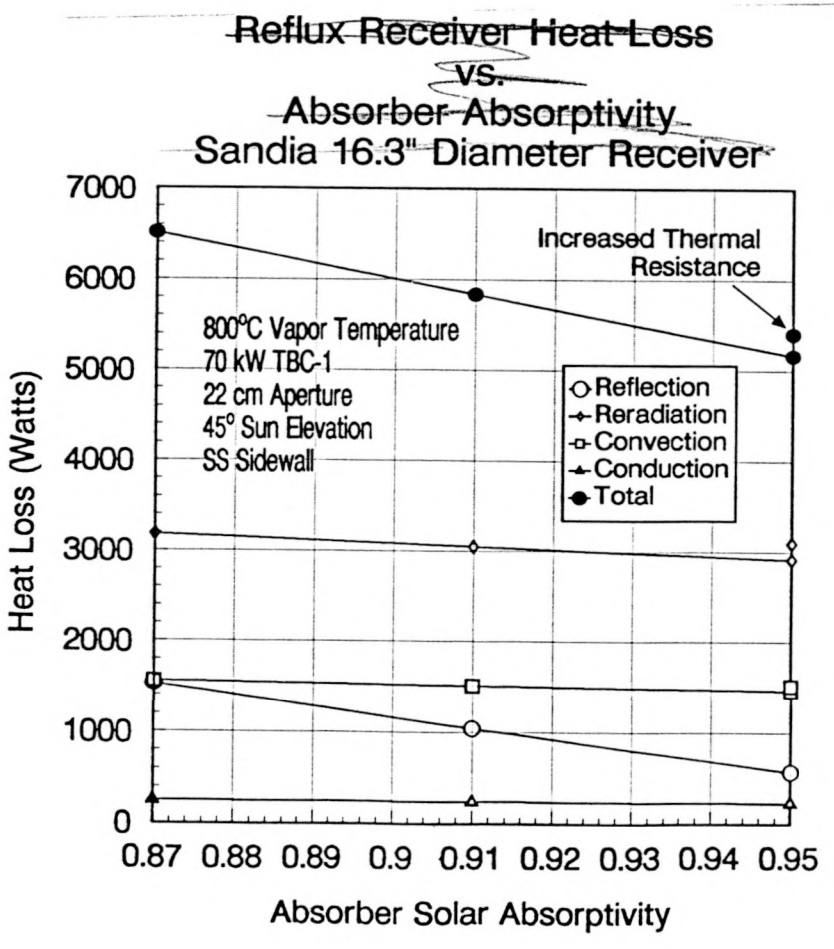

Fig 10

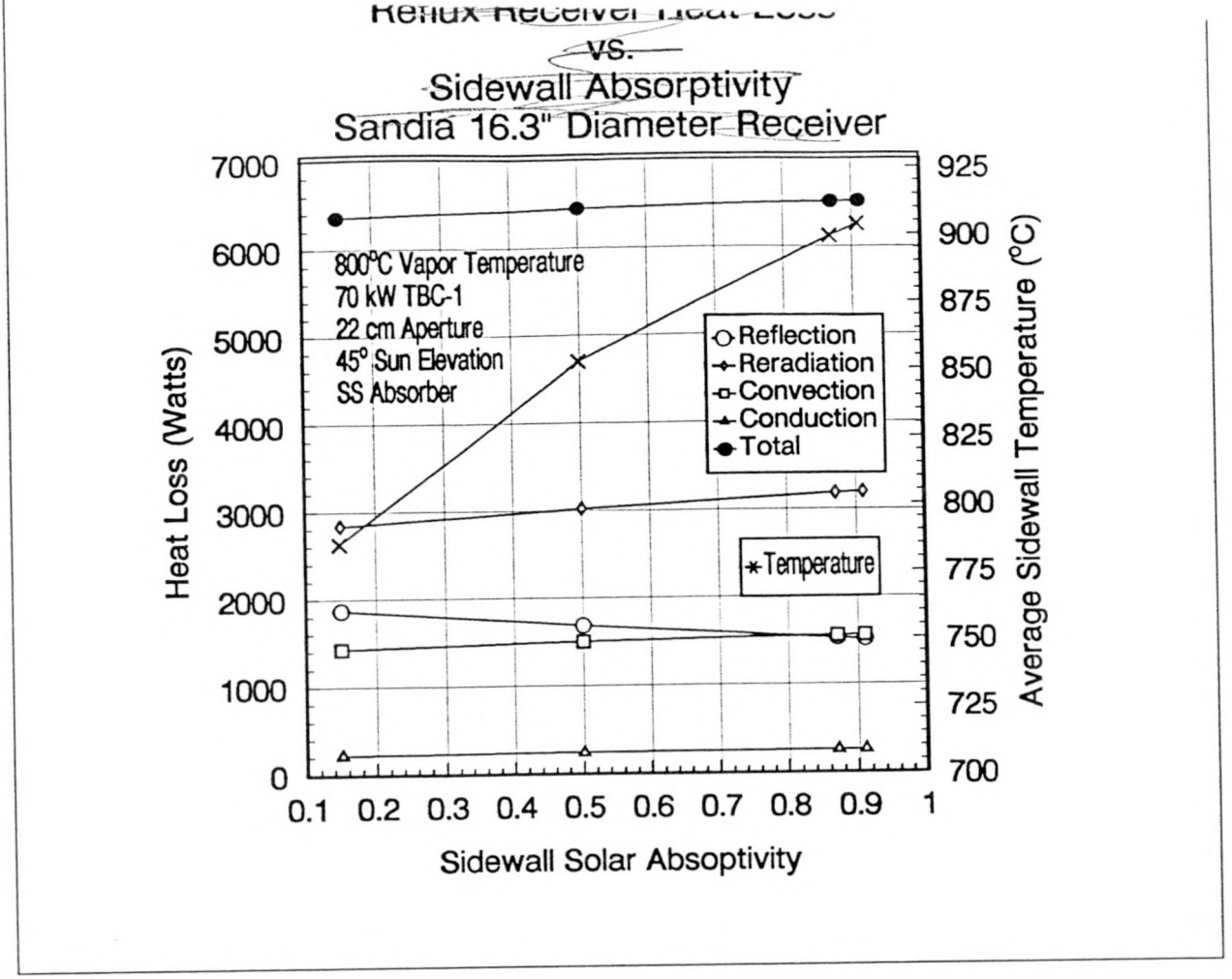

Fig 11 IV_SWMAT

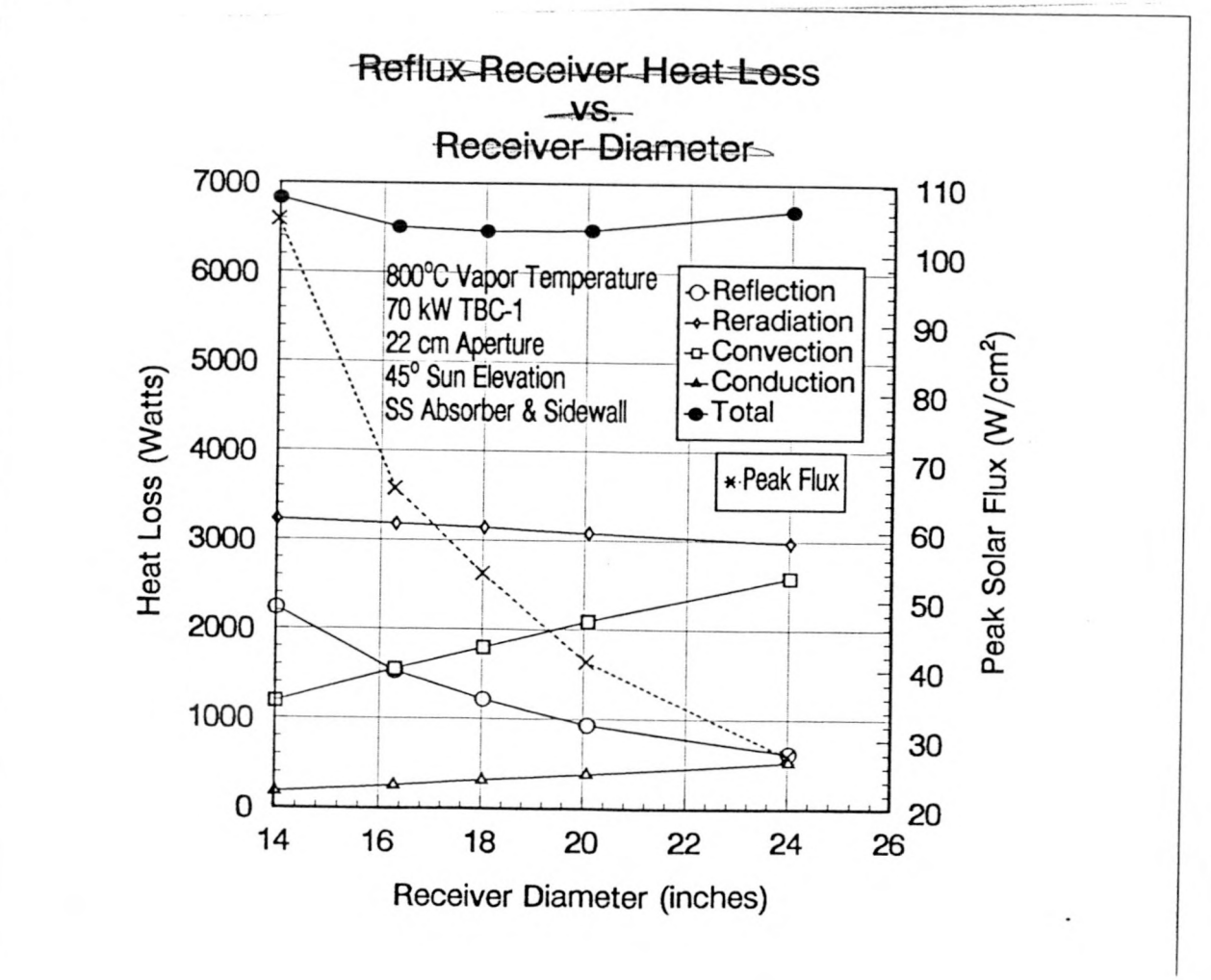

Fig 12

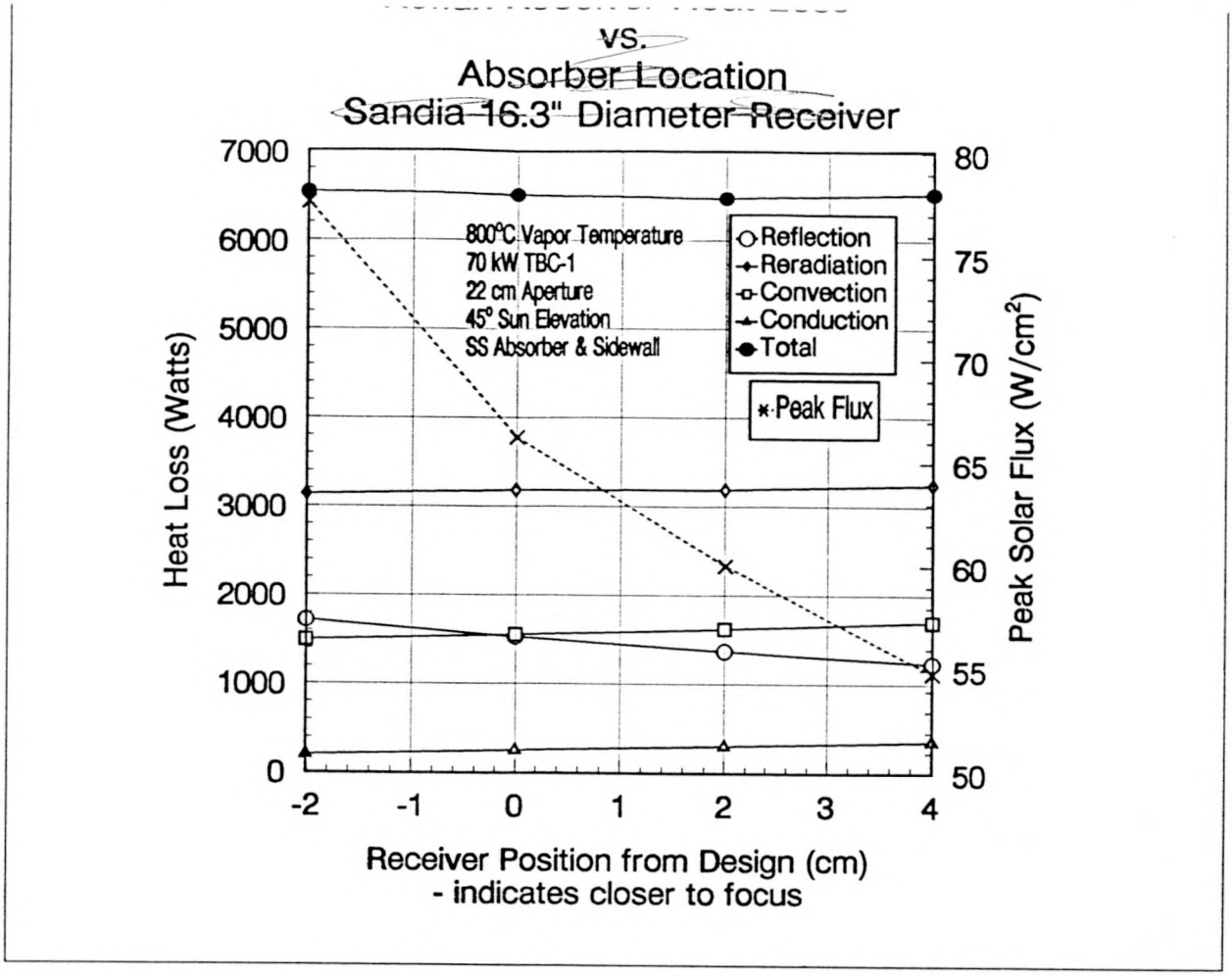

Fig 13 IFRECLOC

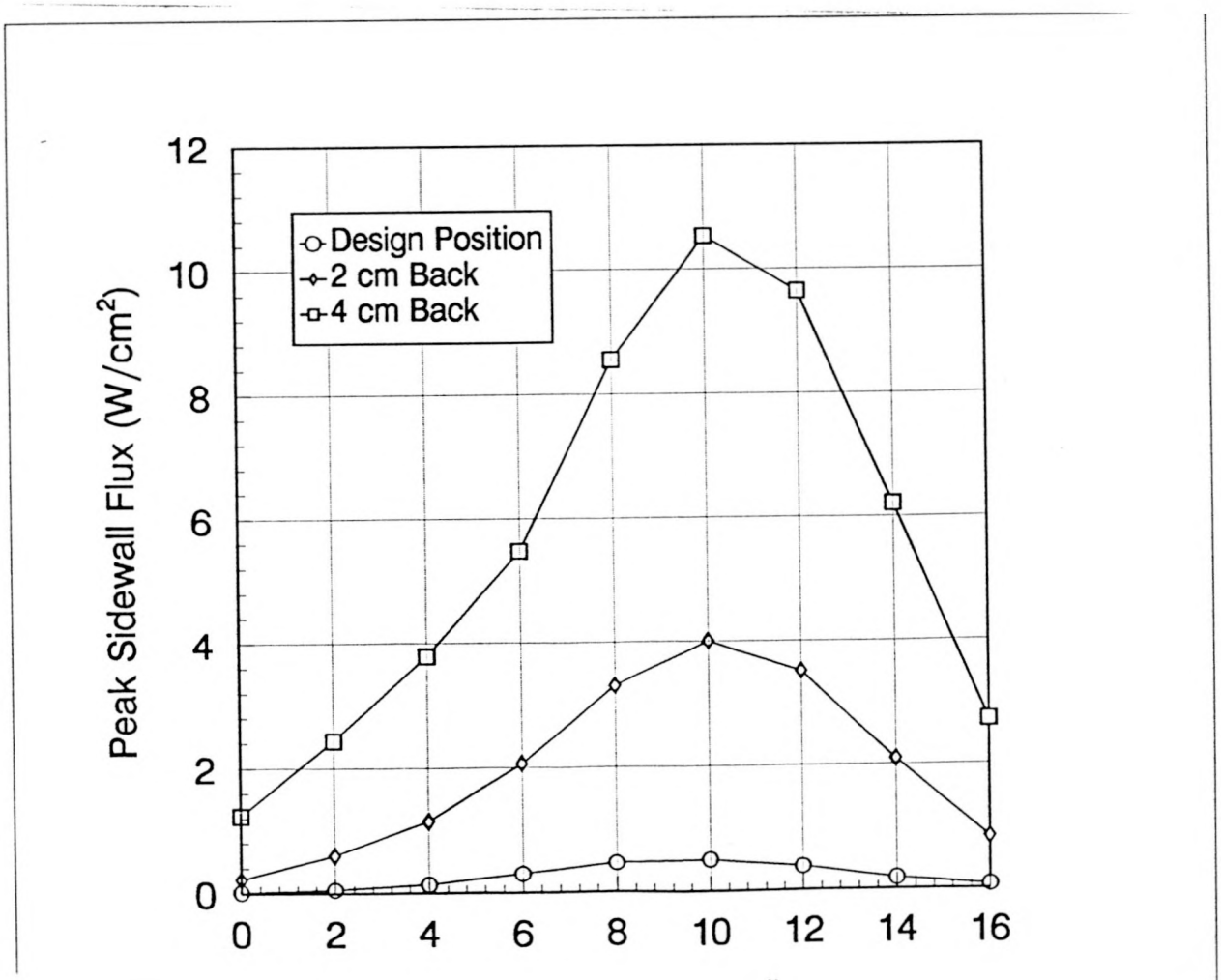

Fig 14

TABLE 1 - REFLUX RECEIVER THERMAL PERFORMANCE PARAMETERS

RECEIVER GEOMETRY	Design Point	Range Analyzed
Receiver Diameter (m)	0.414	.356 to .610
Sphere Angle (degrees)	71	71
Side Wall Angle (degrees)	45	52 to 35
Absorber Thickness (mm)	0.813	0.813
Insulation Thickness (cm)	15.24	15.24
RECEIVER MATERIALS	SS316L	Range Analyzed
Working Fluid h (W/m^2-K)	1x10^8	1x10^8
Absorber Conductivity (W/m-K)	24.5	24.5
Absorber Absorptance (solar)	0.87	0.87 to 0.95
Absorber Emittance (infrared)	0.85	0.85
Side Wall Absorptance (solar)	0.87	0.15 to 0.91
Side Wall Emittance (infrared)	0.85	0.8 to 0.85
Insulation Conductivity (W/m-K)	0.4	0.4
ENVIRONMENTAL PARAMETERS	Stine Convection	Stine Convection
Ambient Temperature (K)	287	287
Sun Elevation Angle (degrees)	45	0 to 90
Wind Speed (mph)	0	0
Wind Direction	-	-
SYSTEM PARAMETERS	Design Point	Range Analyzed
Temperature (C)	800	650 to 850
Flux Distribution	TBC-1	Several
Aperture Size (m)	0.22	0.18 to 0.36
Input Power (kW)	70	70

Table 2 - Sandia Pool-Boiler Receiver Performance Summary												
Date (mm/dd/yy)	Time (MST)	Vapor Temp (Deg. C)	Aper. Diam. (m)	Input Power (kW)	Uncer. + or - (kW)	Output Power (kW)	Uncer. + or - (kW)	Heat Loss (kW)	Uncer. + or - (kW)	Wind Speed (m/sec)	Elev. Angle (Deg.)	AEETES Heat Loss (kW)
10/19/89	10:03	800.9	0.22	65.4	1.0	56.6	3.0	8.8	3.2	1.5	38.1	6.9
10/19/89	12:03	801.0	0.22	66.9	1.0	58.7	3.0	8.2	3.2	1.6	44.8	6.4
10/19/89	14:03	800.9	0.22	65.1	1.0	58.1	3.0	7.0	3.2	1.8	35.1	7.0
10/19/89	16:33	800.5	0.22	44.8	1.0	38.8	3.0	6.0	3.2	1.0	9.8	7.4
11/15/89	14:23	800.6	0.22	63.1	1.0	53.2	1.0	9.9	1.4	5.2	25.4	7.5
11/15/89	14:30	800.4	0.22	62.5	1.0	52.6	1.0	9.9	1.4	6.0	24.5	7.5
05/09/90	12:03	800.7	0.26	68.5	1.2	61.0	1.2	7.5	1.7	4.1	72.5	6.9
05/09/90	12:20	750.4	0.26	68.5	1.2	62.2	1.2	6.3	1.7	5.6	72.0	6.2
05/09/90	13:04	800.7	0.26	66.9	1.2	60.2	1.2	6.7	1.7	3.3	67.7	7.0
05/15/90	08:23	800.7	0.26	60.5	1.2	51.9	1.2	8.6	1.7	7.5	39.2	8.2
05/15/90	09:03	800.1	0.26	62.7	1.2	54.7	1.2	8.0	1.7	7.7	47.3	7.8
05/15/90	09:56	800.6	0.26	64.1	1.2	56.0	1.2	8.1	1.7	1.5	57.8	7.2
05/18/90	09:07	799.7	0.26	60.3	1.2	52.2	1.0	8.1	1.6	2.3	48.5	7.6
05/18/90	09:24	800.7	0.26	61.2	1.2	53.0	1.0	8.2	1.6	4.0	51.9	7.4
05/23/90	09:06	800.4	0.26	61.4	1.2	51.9	1.2	9.5	1.7	3.7	48.7	7.5
05/23/90	09:20	800.5	0.26	57.0	1.2	47.7	1.2	9.3	1.7	3.1	51.5	7.2
05/23/90	10:23	800.7	0.26	63.4	1.2	55.0	1.2	8.4	1.7	2.1	63.8	6.9
05/23/90	10:37	800.7	0.26	65.7	1.2	57.3	1.2	8.4	1.7	2.9	66.3	7.0
05/23/90	11:03	800.7	0.26	59.8	1.2	51.6	1.2	8.2	1.7	7.0	70.5	6.6
					Average Heat Loss			8.16				7.17